Stability and Performance Limits of Latency-Prone Distributed Feedback Controllers

Ye Zhao, *Student Member, IEEE*, Nicholas Paine, *Student Member, IEEE*, Kwan Suk Kim, *Student Member, IEEE*, and Luis Sentis, *Member, IEEE*

***Abstract*—Robotic systems are increasingly relying on distributed feedback controllers to tackle complex sensing and decision problems, such as those found in highly articulated human-centered robots. These demands come at the cost of a growing computational burden and, as a result, larger controller latencies. To maximize robustness to mechanical disturbances by maximizing control feedback gains, this paper emphasizes the necessity for compromise between high- and low-level feedback control efforts in distributed controllers. Specifically, the effect of distributed impedance controllers is studied, where damping feedback effort is executed in close proximity to the control plant and stiffness feedback effort is executed in a latency-prone centralized control process. A central observation is that the stability of high-impedance distributed controllers is very sensitive to damping feedback delay but much less to stiffness feedback delay. This study pursues a detailed analysis of this observation that leads to a physical understanding of the disparity. Then, a practical controller breakdown gain rule is derived to aim at enabling control designers to consider the benefits of implementing their control applications in a distributed fashion. These considerations are further validated through the analysis, simulation, and experimental testing on high-performance actuators and on an omnidirectional mobile base.**

***Index Terms*—Distributed feedback control, feedback delays, high-impedance control, mobile robotics.**

I. Introduction

As a result of the increasing complexity of robotic control systems, such as human-centered robots [1]–[3] and industrial surgical machines [4], new system architectures, particularly distributed control architectures [5], [6], are often being sought for communicating with and controlling the numerous device subsystems. Often, these distributed control architectures manifest themselves in a hierarchical control fashion, where a centralized controller can delegate tasks to subordinate local controllers (see Fig. 1). As it is known, communication between actuators and their low-level controllers can occur at high rates, while communication between low- and high-level controllers occurs more slowly. The latter is further slowed down by the fact that centralized controllers tend to implement larger computational operations, for instance to compute system models or coordinate transformations online.

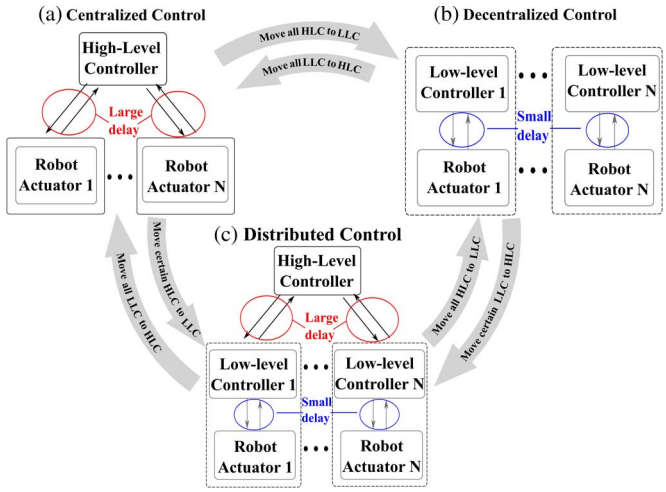

Fig. 1. Depiction of various control architectures. Many control systems today employ one of the control architectures shown: (a) Centralized control with only high-level feedback controllers (HLCs); (b) Decentralized control with only low-level feedback controllers (LLCs); (c) Distributed control with both HLCs and LLCs, which is the focus of this paper.

A. Control Architectures With Feedback Delays

One concern is that feedback controllers with large delays, such as the centralized controllers mentioned earlier, are less stable than those with small delays, such as locally embedded controllers. Without the fast servo rates of embedded controllers, the gains in centralized controllers can only be raised to limited values, decreasing their robustness to external disturbances [7] and unmodeled dynamics [8].

As such, why not remove centralized controllers altogether and implement all feedback processes at the low level? Such operation might not always be possible. For instance, consider

Manuscript received January 9, 2015; revised April 23, 2015; accepted May 15, 2015. Date of publication June 23, 2015; date of current version October 7, 2015. This work was supported by NASA through the National Robotics Initiative under Grant NNX12AM03G.

Y. Zhao, K. S. Kim, and L. Sentis are with the Department of Mechanical Engineering, The University of Texas at Austin, Austin, TX 78712 USA (e-mail: yezhao@utexas.edu; kskim@utexas.edu; lsentis@austin.utexas.edu).

N. Paine is with the Department of Electrical and Computer Engineering, The University of Texas at Austin, Austin, TX 78712 USA (e-mail: npaine@utexas.edu).

Color versions of one or more of the figures in this paper are available online at http://ieeexplore.ieee.org.

Digital Object Identifier 10.1109/TIE.2015.2448513

controlling the behavior of human-centered robots (i.e., highly articulated robots that interact with humans). Normally, this operation is achieved by specifying the goals of some task frames such as the end-effector coordinates. One established option is to create impedance controllers on those frames and transform the resulting control references to actuator commands via operational space transformations [9]. Such a strategy requires the implementation of a centralized feedback controller, which can utilize global sensing data, access the state of the entire system model, and compute the necessary models and transformations for control. Because of the aforementioned larger delays on high-level controllers, does this imply that high-gain control cannot be achieved in human-centered robot controllers due to stability problems? It will be shown that this may not need to be the case, but for now, this delay issue is one of the reasons why various currently existing human-centered robots cannot achieve the same level of control accuracy that is found in high-performance industrial manipulators. More concretely, this study proposes a distributed impedance controller where only proportional (i.e., stiffness) position feedback is implemented in the high-level control process with slow servo updates. This process will experience the long latencies found in many modern centralized controllers of complex human-centered robots. At the same time, it contains global information of the model and the external sensors that can be used for operational space control. For stability reasons, our study proposes to implement the derivative (i.e., damping) position feedback part of the controller in low-level embedded actuator processes, which can therefore achieve the desired high update rates.

B. Analysis of Sensitivity to Delay

To focus the study on the physical performance of the proposed distributed control approach, our study first focuses on a single-actuator system with separate stiffness and damping servos and under multiple controller delays. Then, the physical insights gained are used as a basis for achieving high-impedance behaviors in single-actuator systems and in an omnidirectional mobile base. Let us pose some key questions regarding distributed stiffness–damping feedback controllers considered in this study: 1) Does controller stability have different sensitivity to stiffness and damping feedback delays? 2) If that is the case, what are the physical reasons for such a difference?

To answer these questions, this paper studies the physical behavior of the proposed real-time distributed system using control analysis tools, such as the phase margin stability criterion, applied to the system's plant. Using these tools, our study reveals that system closed-loop stability and performance are much more sensitive to damping feedback delays than to stiffness feedback delays.

C. Benefits of the Proposed Distributed Control Architecture

As it will be empirically demonstrated, the benefit of the proposed split control approach over a monolithic controller implemented at the high level is to increase control stability due to the reduced damping feedback delay. As a direct result, closed-loop actuator impedance may be increased beyond the levels possible with a monolithic high-level impedance controller. This conclusion may be leveraged on many practical systems to improve disturbance rejection by increasing gains without compromising overall controller stability. As such, these findings are expected to be immediately useful on many complex human-centered robotic systems.

To demonstrate the effectiveness of the proposed methods, this study implements tests on a high-performance actuator followed by experiments on a mobile base. First, a position step response is tested on an actuator under various combinations of stiffness and damping feedback delays. The experimental results show high correlation to their corresponding simulation results. Second, the proposed distributed controller is applied to an implementation into an omnidirectional base. The results show a substantial increase in closed-loop impedance capabilities, which results in higher tracking accuracy with respect to the monolithic centralized controller counterpart approach.

Consequently, our main contribution is to analyze, provide control system solutions, implement, and evaluate actuators and mobile robotic systems with latency-prone distributed architectures to significantly enhance their stability and trajectory tracking capabilities. In particular, a new study is performed to reveal that system stability and performance are more sensitive to damping servo latencies than stiffness servo latencies. Then, a novel servo breakdown rule is proposed to evaluate the benefits of using a distributed control architecture. As a conclusion, this paper proposes using stiffness servos for centralized operational space control, while realizing embedded-level damping servos as joint-space damping processes for stability and tracking accuracy.

This paper is organized as follows: related work of our study is presented in Section II; Then, Section III proposes a distributed control architecture, which is simulated with observations of phase margin sensitivity to feedback delays. Then, the fundamental reasons of this sensitivity discrepancy are analyzed in detail, and a servo breakdown gain rule is proposed correspondingly in Section IV. To validate this discrepancy, experimental evaluations are shown in Section V. Finally, Section VI concludes this study and discusses future directions.

II. Related Work

Advances in distributed control technologies [6], [10], [11] have enabled the development of decentralized multiple–input–and–multiple–output systems such as humanoid systems and highly articulated robots [2], [3], [12]. Distributed control architectures combine centralized processes with self-contained control units that are in close proximity to actuators and sensors. In [5], servo motor controllers are used as subcontrollers coordinated via control area network (CAN) communications by a central controller. As a result, computation burden on the central controller is reduced based on this distributed architecture. Recently, a distributed motion control system [13] has been developed to experimentally demonstrate the capabilities of real-time communications and synchronous tracking control. Analogous to human muscle actuation and neural systems, a bio-inspired distributed control infrastructure [14] reduces

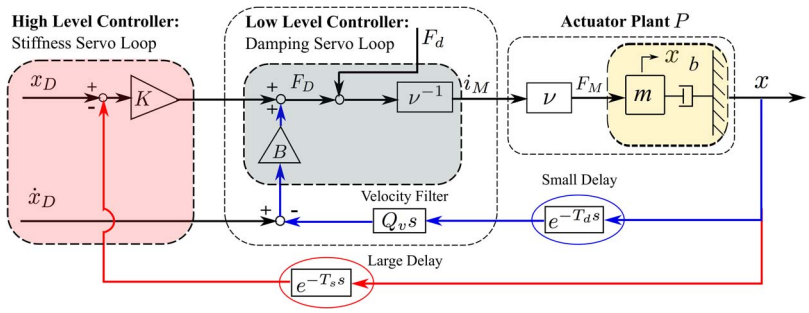

Fig. 2. Single-input/single-output controller with distributed structure. A simple PD control law is used to control an actuator. P denotes the actuator plant with motor current input i_M and position output x. ν^{-1} represents a scaling constant mapping the desired force F_D to the motor current i_M. K is the stiffness feedback gain, while B is the damping feedback gain.

controller task complexity by offloading parts of the controller into the robot's limb processors. Another typical distributed control architecture, which is related to neuroscience and robotics, is locomotor central pattern generators (CPGs) [15], [16]. CPGs are modeled as distributed neural networks of multiple coupled oscillators to control articulated robot locomotion. This distributed architecture has the advantage of reducing time delays in the motor control loop (i.e., fast feedback loops through the spinal cord), in order to efficiently coordinate mechanical movements with rhythms.

However, the effect on controller performance due to the ever-growing computational demand on feedback servos and latency-prone serial communications in human-centered robots has been largely overlooked on distributed controller studies. A detailed analysis, exploration, and implementation of the high-impedance capabilities of distributed controllers with latency-prone centralized processors have not been previously performed. To this end, our study focuses on how a distributed controller improves control system stability and performance over monolithic centralized control approaches.

Robustness and effects of delay have often been studied in work regarding proportional–integral–derivative (PID) controller tuning. A survey of PID controllers, including system plants using phase margin techniques with linear approximations, is conducted in [17]. The works in [18] and [19] study autotuning and adaption of PID controllers, while the work in [20] furthers these techniques by developing optimal design tools applied to various types of plants, which include delays. The study in [21] proposed an optimal gain scheduling method for dc motor speed control with a PI controller. In [22], a backstepping controller with time-delay estimation and nonlinear damping is considered for variable PID gain tuning under disturbances. The high volume of studies on PID tuning methods highlights the importance of this topic for robust control under disturbances. However, neither do those studies consider the sensitivity discrepancy to latencies between the stiffness and damping servos as separate entities nor do they consider the decoupling of those servos into separate processes for stability purposes, as it is done in this paper.

The field of haptics [23], networked control [24]–[26], sensing [27], and teleoperation [21] have also thoroughly studied delays and filtering effects. Due to the destabilizing effects of time delays, significant effort has been put forth to ensure that systems are stable, by enforcing passivity criteria [23]. The work in [28] further relaxes this constraint and focuses on how delay and filtering affect stability. In parallel to these model-based approaches aforementioned, recent data-driven techniques [29], [30] provide promising alternatives to solve delay and filtering issues in complicated industrial applications. Once more, these studies neither analyze nor exploit the large sensitivity discrepancy between stiffness and damping feedback loops nor propose solutions to increase performance based on this discrepancy.

III. Basic Distributed Control Structure

This section describes the actuator model used to analyze closed-loop system stability, proposes a basic distributed control architecture that delocalizes stiffness and damping servo loops, and analyzes the sensitivity of these control processes to loop delays.

A. Actuator Plant Model

Many rigid electrical actuators, such as those used in modern robots, can be approximately modeled as a second-order plant with a force acting on an inertia-damper pair (as shown in Fig. 2).

Considering a current-controlled motor, the control plant from current i_M to position x is given by

$$P(s) = \frac{x(s)}{i_M(s)} = \frac{x(s)}{F_M(s)} \frac{F_M(s)}{i_M(s)} = \frac{\nu}{ms^2 + bs} \tag{1}$$

where F_M is the applied motor force, $\nu \triangleq F_M/i_M = \eta N k_\tau$, η is the drivetrain efficiency, N is the gear speed reduction, and k_τ is the motor torque constant.

B. Closed-Loop Distributed Controller Model

Fig. 2 shows our proposed distributed controller built using a PD feedback mechanism. It includes velocity feedback filtering $(Q_v s)$; stiffness feedback delay (T_s); damping feedback delay (T_d), with $T_s \neq T_d$; stiffness feedback gain (K); and damping feedback gain (B). Excluding the unknown load (F_d), the desired motor force (F_D) in the Laplace domain associated with the proposed distributed controller is given by

$$F_D(s) = K(x_D - e^{-T_s s}x) + B(x_D s - e^{-T_d s} Q_v x s) \tag{2}$$

where s is the Laplace variable, x_D and $\dot{x}_D$ (i.e., $x_D s$ in the Laplace domain) are the desired output position and velocity, and $e^{-T_s s}$ and $e^{-T_d s}$ represent Laplace transforms of the time delays in the stiffness and damping feedback loops, respectively. Using (1) and (2), one can derive the closed-loop transfer function from desired to output positions as

$$P_{\mathrm{CL}}(s) = \frac{x}{x_D} = \frac{Bs + K}{ms^2 + (b + e^{-T_d s} BQ_v)s + e^{-T_s s} K} \quad (3)$$

where Q_v is chosen to be a first-order low-pass filter with a cutoff frequency f_v. That is,

$$Q_v(s) = \frac{2\pi f_v}{s + 2\pi f_v}. \quad (4)$$

To derive the open-loop transfer function [32] of the distributed controller, one can rewrite (3) as

$$P_{\mathrm{CL}}(s) = \frac{\frac{Bs+K}{ms^2+bs}}{1 + P_{\mathrm{OL}}(s)} \quad (5)$$

where $P_{\mathrm{OL}}(s) \triangleq P(s)H(s)$ is the open-loop transfer function. That is,

$$P_{\mathrm{OL}}(s) = \frac{e^{-T_d s} BQ_v s + e^{-T_s s} K}{ms^2 + bs}. \quad (6)$$

$P(s)$ is the actuator's plant, and $H(s)$ is the so-called feedback transfer function.

The presence of delays and filtering causes the aforementioned closed-loop plant to behave as a high-order dynamic system, for which typical gain selection methods do not apply. However, to make the problem tractable, one can define a dependence between the stiffness and damping gains using an idealized second-order characteristic polynomial [32]

$$s^2 + 2\zeta\omega_n s + \omega_n^2 \quad (7)$$

where ω_n is the so-called natural frequency, and ζ is the so-called damping factor. In such case, the idealized characteristic polynomial [i.e., ignoring delays ($T_s = T_d = 0$) and filtering ($Q_v = 1$)] associated with our closed-loop plant of (3) would be

$$s^2 + (B + b)/m \cdot s + K/m. \quad (8)$$

Choosing the second-order critically damped rule $\zeta = 1$ and comparing (7) and (8), one can get the gain dependence

$$B = 2\sqrt{mK} - b \quad (9)$$

and the natural frequency

$$f_n \triangleq \frac{\omega_n}{2\pi} = \frac{1}{2\pi}\sqrt{\frac{K}{m}}. \quad (10)$$

The second-order dependence of (9) will be used, for the remainder of this paper, for deriving new gain selection methods through the thorough analysis of the oscillatory behavior of the closed-loop plant of (3). In particular, our study will use the phase margin criterion and other visualization tools to study how the complete system reacts to feedback delays and signal filtering. Phase margin is the additional phase value above $-180°$ when the magnitude plot crosses the 0-dB line (i.e., the gain crossover frequency). It is common to quantify system stability by its phase margin.

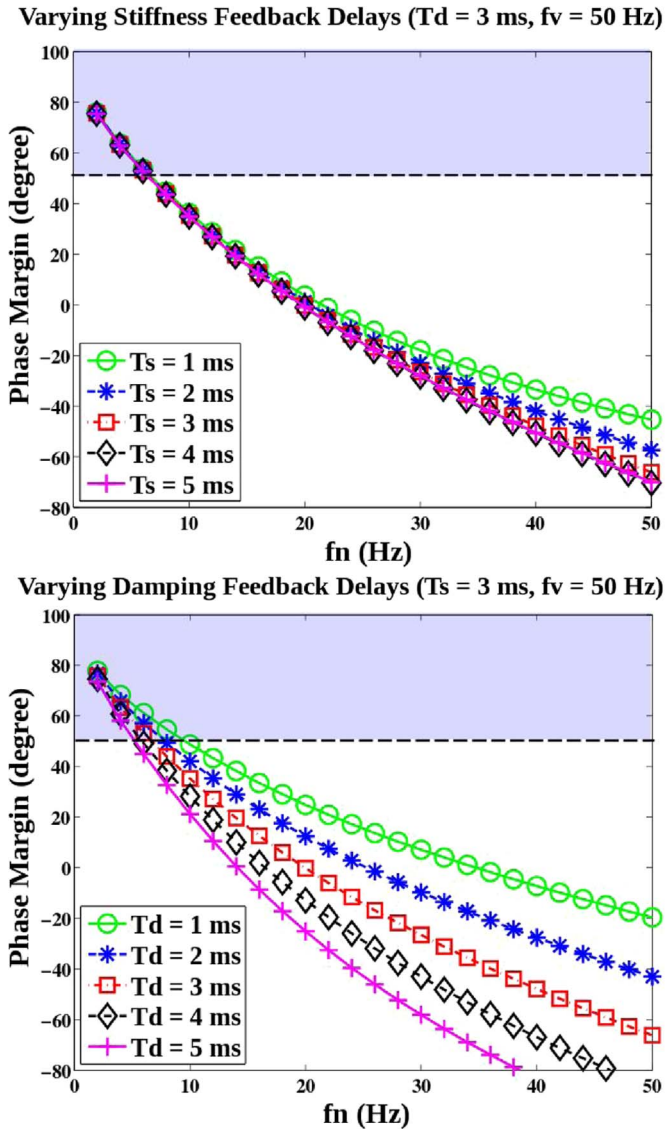

Fig. 3. Phase margin sensitivity to loop delays. This figure shows phase margin simulations of the open-loop transfer function shown in (6) as a function of the natural frequency defined in (10) and the servo delays shown in Fig. 2. A phase margin of 0° is considered marginally stable. Simulations indicate that phase margins less than 50° exhibit oscillatory behavior [31]. The dashed line in this figure represents this threshold.

For the proposed distributed controller in Fig. 2, the damping feedback loop is labeled as low level (e.g., embedded) to emphasize that it is meant to be locally implemented to take advantage of high servo rates. On the other hand, the stiffness loop is implemented in a high-level computational process close to external sensors and centralized models, for operational space control purposes. Operational space control is normally used in human-centered robotic applications, where controllers use task coordinates and global models for their operation. The simplified controller in Fig. 2 is used to illustrate the discrepancies in sensitivity to latencies between the servo

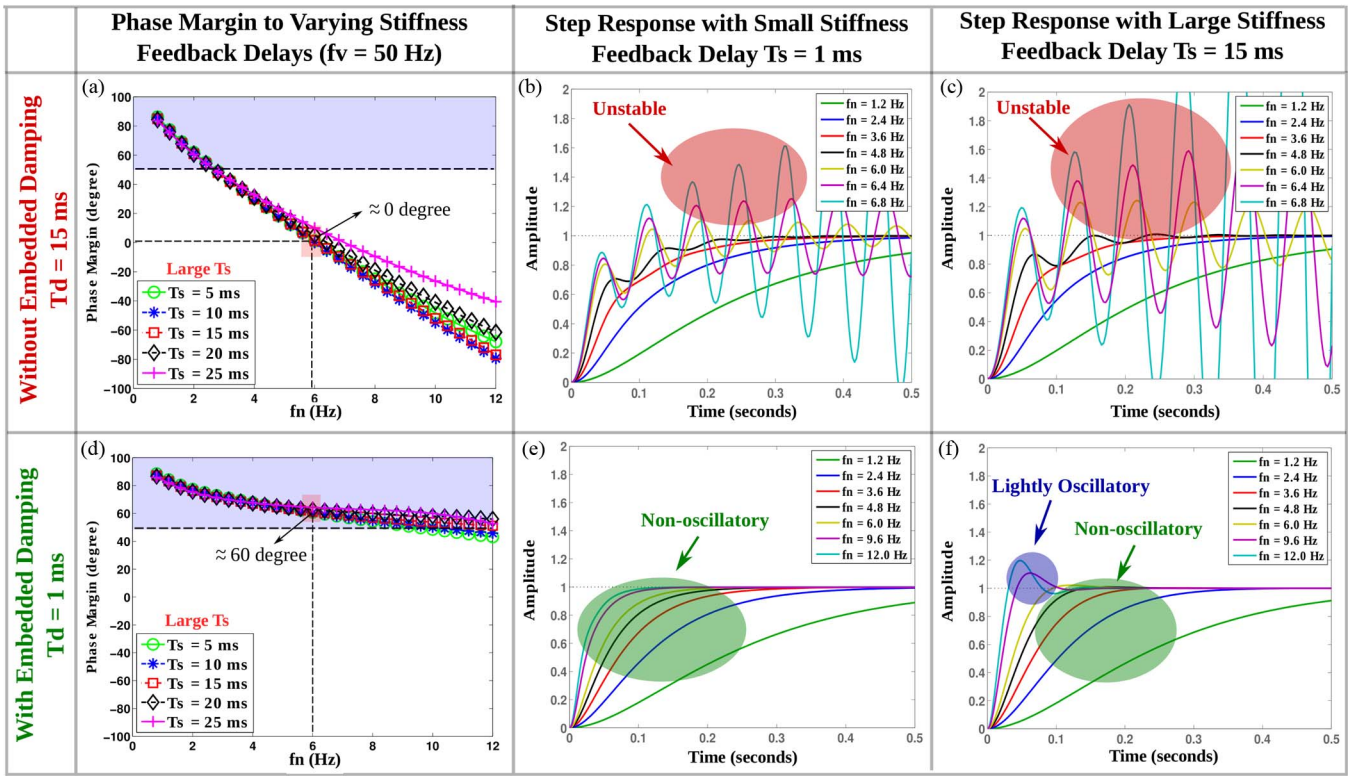

Fig. 4. Comparison between step responses with slow and fast damping servos. These subfigures compare the effects of damping feedback on slow or fast servo processes. The simulations are performed on the same actuator used in the experimental section in Section V. The top row depicts damping feedback implemented with delays of 15 ms, while the bottom row depicts a faster damping servo with delay of only 1 ms. For both rows, various stiffness delays are identically used ranging from 5 to 25 ms. (a) and (d) Simulations of the phase margin once more as a function of the natural frequency, which in turn is a function of the feedback stiffness gain.

loops. It does not correspond to a practical robot controller as it contains only a single degree of freedom. After analyzing this structure, we implement a similar distributed controller into a multiaxis robotic base shown in Fig. 8, which results in the simultaneous improvement in system stability while achieving operational space control.

C. Phase Margin Sensitivity Comparison

This subsection focuses on utilizing frequency-domain control methods to analyze the phase margin sensitivity to time delays on the distributed control architecture shown in Fig. 2. Different delay range scales are considered: 1) a small range scale (1–5 ms) to show detailed variations and 2) a larger range scale (5–25 ms) to cover practical delay ranges. These scales roughly correspond to embedded and centralized computational and communication processes found in highly articulated robots such as [1]. Phase margin plots are subsequently obtained for the controller of (3) and shown in Figs. 3 and 4 as a function of the natural frequency given in (10) and using the gain relationship of (9). All the simulations are carried out using MATLAB software. Feedback delays are represented by the exponential term e^{-Ts} in the frequency domain. Phase margin is computed by using MATLAB's margin() command based on the open-loop transfer function.

In Fig. 3, delays ranging between 1 and 5 ms are simulated for both the stiffness and damping servos. The simulations are performed based on identical actuator parameters to those used in the experimental section in Section V, i.e., passive output inertia $m = 256$ kg and passive damping $b = 1250$ Ns/m. Equations (9) and (10) can subsequently be used to derived the stiffness and damping feedback gains. It is noticeable that reducing either stiffness or damping feedback delays will increase the stability of the controller, but more importantly, it is clearly visible that phase margin behavior is much more sensitive to damping servo delays (T_d) than to stiffness servo delays (T_s). Not only is there a disparity on the behavior with respect to the delays, but the phase margin also is fairly insensitive to stiffness servo delays in the observed time scales. Such disparity and behavior is the central observation that motivates this paper and the proposed distributed control architecture. Fig. 4 simulates step position responses of the controller for a range of relatively large stiffness delays and for two choices of damping delays, i.e., a short and a long one. The first point to notice here is that the phase margin values for subfigure (a) are significantly lower than for (d) due to the larger damping delay. Second, both (a) and (d) show small variations between the curves, corroborating the small sensitivity to stiffness delays that will be studied in Section IV. Corresponding step responses are shown along for various natural frequencies. It becomes clear that reducing damping delay significantly boosts stability even in the presence of fairly large stiffness delays. These results emphasize the significance of implementing damping terms at the fastest possible level (e.g., at the embedded level), while

proportional (i.e., stiffness) servos can run in latency-prone centralized processes. This conclusion is also validated by the Nichols diagram [33].

IV. Basis for Sensitivity Discrepancy

In the previous section, different behavior of the controller's phase margin depending on the nature of delay was observed. Damping delay seems to affect much more the system's phase margin than stiffness delay. This section will analyze this physical phenomenon in much more detail and reveal the conditions under which this disparity occurs.

A. Equations Expressing Phase Margin Sensitivity to Delays

A detailed mathematical analysis is developed to find further physical structure for the causes of stability discrepancies between damping and stiffness delays. Let us revisit the open-loop transfer function of (6). The resulting open-loop transfer function, including the low-pass velocity filter of (4), in the frequency domain ($s = j\omega$) is given by

$$P_{\mathrm{OL}}(\omega) = \frac{jA_1(\omega) + A_2(\omega)}{j\omega(jm\omega + b)(j\tau_v\omega + 1)} \tag{11}$$

with

$$\begin{aligned} A_1(\omega) &\triangleq B\,\omega\,\cos(T_d\,\omega) - K\,\sin(T_s\,\omega) + K\tau_v\omega\,\cos(T_s\omega) \\ A_2(\omega) &\triangleq B\,\omega\,\sin(T_d\,\omega) + K\,\cos(T_s\,\omega) + K\tau_v\omega\,\sin(T_s\omega). \end{aligned} \tag{12}$$

Note that Euler's Formula ($e^{-jx} = \cos x - j\sin x$) has been used to obtain the aforementioned results.

The phase margin $\mathrm{PM} \triangleq 180^\circ + \angle P_{\mathrm{OL}}(\omega_g)$ of the plant (11), where $\angle$. is the angle of the argument, is given by

$$\mathrm{PM} = \mathrm{atan}\left[\frac{A_{1g}}{A_{2g}}\right] + 90^\circ - \mathrm{atan}\left[\frac{m\,\omega_g}{b}\right] - \mathrm{atan}[\tau_v\omega_g] \tag{13}$$

with ω_g being the gain crossover frequency [32] and $A_{ig} \triangleq A_i(\omega_g), i = \{1, 2\}$. After performing several manipulations (details are ignored due to space constraints), we obtain the following sensitivity equations expressing variations of the phase margin with respect to stiffness and damping delays:

$$\frac{\partial \mathrm{PM}}{\partial T_s} = \frac{\left[-K^2(\tau_v^2\omega_g^2 + 1) + K\,B\,\omega_g\,M\right]\,\omega_g}{A_{1g}^2 + A_{2g}^2} \tag{14}$$

$$\frac{\partial \mathrm{PM}}{\partial T_d} = \frac{\left[-B^2\omega_g^2 + K\,B\,\omega_g\,M\right]\,\omega_g}{A_{1g}^2 + A_{2g}^2} \tag{15}$$

where

$$M = \sqrt{(\tau_v\omega_g)^2 + 1}\cdot\sin\left((T_s - T_d)\,\omega_g + \phi\right) \tag{16}$$

where the phase shift $\phi \triangleq \mathrm{atan}(-\tau_v\omega_g)$.

B. Gain Crossover Sensitivity Condition

From the control analysis of the distributed plant performed in previous sections, increasing damping delays decreases the phase margin. This observation means that the sensitivity of the phase margin to damping delays must be negative, i.e.,

$$\frac{\partial \mathrm{PM}}{\partial T_d} < 0. \tag{17}$$

In addition, from those analysis, it is observed that the phase margin is more sensitive to damping than to stiffness delays. This observation can be formulated as

$$\frac{\partial \mathrm{PM}}{\partial T_d} < \frac{\partial \mathrm{PM}}{\partial T_s}. \tag{18}$$

Let us reorganize the numerator of (15) to be written in the alternate form

$$\frac{\partial \mathrm{PM}}{\partial T_d} = \frac{[-B\omega_g + KM]B\,\omega_g^2}{A_{1g}^2 + A_{2g}^2}. \tag{19}$$

An upper bound of the aforementioned equation occurs when the maximal condition $\sin((T_s - T_d)\,\omega_g + \phi) = 1$ is met, i.e.,

$$\frac{\partial \mathrm{PM}}{\partial T_d} \leq \frac{\left[-B\omega_g + K\sqrt{(\tau_v\omega_g)^2 + 1}\right]B\,\omega_g^2}{A_{1g}^2 + A_{2g}^2}. \tag{20}$$

Based on the aforementioned inequality, (17) is met if the following gain crossover sensitivity condition is met:

$$\omega_g > \frac{K}{\sqrt{B^2 - K^2\tau_v^2}}. \tag{21}$$

The aforementioned equation is only a sufficient condition for fulfilling condition (17). Obtaining a closed-form solution for that condition would be very complex due to the presence of trigonometric terms. Therefore, the remainder of this section is to study under what circumstances condition (21) holds.

At the same time, inequality (18) can be rewritten in the form

$$\frac{\partial \mathrm{PM}}{\partial T_d} - \frac{\partial \mathrm{PM}}{\partial T_s} = \frac{\left[-B^2\omega_g^2 + K^2\left(\tau_v^2\omega_g^2 + 1\right)\right]\omega_g}{A_{1g}^2 + A_{2g}^2} < 0 \tag{22}$$

where it has been subtracted the right-hand sides of (14) and (15) for the derivation. Notice that, in that subtraction, the sine functions cancel out. Coincidentally, the aforementioned inequality is also met if the gain crossover sensitivity condition (21) is fulfilled. In other words, that condition is sufficient to meet both inequalities (17) and (18).

C. Servo Breakdown Gain Rule

To validate the gain crossover condition (21), this study solves for the gain crossover frequency, which consists of the frequency at which the magnitude of the open-loop transfer function is equal to unity, i.e.,

$$|P_{\mathrm{OL}}(\omega_g)| = 1. \tag{23}$$

Using the plant (11), it can be shown (once more, we omit the manipulations due to space constraints) that the aforementioned equation results in the equality

$$(B\omega_g)^2 + K^2(\tau_v^2\omega_g^2 + 1) - 2KB\omega_g M = \omega_g^2\left((\omega_g m)^2 + b^2\right)\left(\tau_v^2\omega_g^2 + 1\right). \quad (24)$$

The aforementioned equation is intractable in terms of deriving a closed-loop expression of the gain crossover frequency. To tackle a solution, this study introduces transformations of the parameters and numerically derives parameter ranges for which condition (21) holds. Let us start by creating a new variable that allows writing (21) as an equality

$$\delta \in [-1, \infty) \quad \text{s.t.} \quad \omega_g = (1+\delta)\frac{K}{\sqrt{B^2 - K^2\tau_v^2}}. \quad (25)$$

Thus, demonstrating the gain crossover sensitivity condition (21) is equivalent to demonstrating that $\delta > 0$. Rewriting (9) as $K = (B+b)^2/4m$ and substituting K in the aforementioned equation, (25) can be further expressed as

$$\omega_g = (1+\delta)\frac{(B+b)^2}{\sqrt{16B^2m^2 - (B+b)^4\tau_v^2}}. \quad (26)$$

Dividing (24) by a new term $K^2\,U\,V$, with $U \triangleq \tau_v^2\omega_g^2 + 1$ and $V \triangleq B^2\,\omega_g^2/K^2$, while substituting ω_g on the right-hand side of (24) by (26), and using M as shown in (16), (24) becomes

$$\frac{1}{U} + \frac{1}{V} - \frac{2\sin\left((T_s - T_d)\,\omega_g + \phi\right)}{\sqrt{U\cdot V}} = \frac{(1+\delta)^2\,(B+b)^4}{16\,B^4 - B^2(B+b)^4\tau_v^2/m^2} + \left(\frac{b}{B}\right)^2. \quad (27)$$

Using (25), it can be further demonstrated that $V = (\tau_v\omega_g)^2 + (1+\delta)^2$. Thus, U and V are only expressed in terms of $(\tau_v\omega_g)^2$. To further facilitate the analysis, let us introduce three more variables

$$\alpha \triangleq \sin\left((T_s - T_d)\,\omega_g + \phi\right) \in [-1, 1] \quad (28)$$

$$\beta \in (0, \infty) \quad \text{s.t.} \quad B = \beta\, m \quad (29)$$

$$\gamma \in (0, \infty) \quad \text{s.t.} \quad B = \gamma\, b. \quad (30)$$

Notice that α can be interpreted as an uncertainty, β is the ratio between damping gain and motor drive inertia, and γ is the ratio between damping gain and motor drive friction. Using these variables, (27) simplifies to

$$\frac{U + V - 2\alpha\sqrt{U\cdot V}}{U\cdot V} = \frac{(1+\delta)^2\,(1+\gamma)^4}{16\,\gamma^4 - (1+\gamma)^4\beta^2\tau_v^2} + \frac{1}{\gamma^2}. \quad (31)$$

Using (26), (29) and (30), the term $(\tau_v\omega_g)^2$ appearing in the variables U and V on (31) can be expressed as

$$(\tau_v\omega_g)^2 = \beta^2\tau_v^2\frac{(1+\delta)^2\,(1+\gamma)^4}{16\,\gamma^4 - (1+\gamma)^4\beta^2\tau_v^2}. \quad (32)$$

Thus, (31) does not contain direct dependencies with ω_g and therefore can be represented as the nonlinear function

$$f(\alpha, \beta, \gamma, \delta, \tau_v) = 0. \quad (33)$$

Let us demonstrate under which conditions $\delta > 0$, which will imply that (21) holds. In this paper, velocity filters with $\tau_v = 0.0032\,\text{s}$ are commonly used for achieving high-performance control [31], and therefore, (31) will be solved for only that filter. Notice that it is not difficult to try new values of τ_v when needed. Additionally, when sampling (31) for the values of α shown in (28), it is observed that not only δ is fairly invariant to α but also the lowest value of δ occurs for $\alpha = 1$. These behaviors are omitted here for space purposes. Therefore, as a particular solution, (31) is solved for the values

$$f(\alpha = 1, \beta, \gamma, \delta, \tau_v = 0.0032) = 0. \quad (34)$$

The aforementioned function is solved numerically, and the solution surface is plotted in Fig. 5. As it can be seen, $\delta > 0$ for $\gamma > 2$, allowing us to state that using a distributed PD feedback control law, such as the one in Fig. 2, with the particular choice of the filter $\tau_v = 0.0032\,\text{s}$ and with damping gains greater than

$$B > 2\,b \quad (35)$$

causes the phase margin to be more sensitive to damping delays than to stiffness delays. The threshold earlier can therefore be interpreted as a breakdown gain rule, which is sufficient to meet the gain crossover sensitivity condition (21), and from which the aforementioned phase margin sensitivity discrepancy follows.

This threshold hints toward a general rule for breaking controllers down into distributed servos, as was illustrated in Fig. 2. Namely, if the maximum allowable feedback damping gain for a given servo rate is significantly larger than twice the passive actuator damping, then the controller's stiffness servo can be decoupled from the damping servo to a slower computational process without hurting the controller's stability.

In the next section, we study in detail the implementation of the proposed distributed control strategy in a new high-performance linear rigid actuator and an omnidirectional mobile base.

V. Experimental Evaluation

The proposed controller in Fig. 2 is implemented in our linear rigid actuator shown in Fig. 6. This actuator is equipped with a PC-104 form factor computer running Ubuntu Linux with a real-time application interface (RTAI) patched kernel [34]. The PC communicates with the actuator using analog and quadrature signals through a custom signal conditioning board. Continuous signal time derivatives are converted to discrete form using a bilinear Tustin transform written in C. A load arm is connected to the output of the ball screw pushrod. Small displacements enable the actuator to operate in an approximately linear region of its load inertia. At the same time, the controller is simulated by using the closed-loop plant given in (5).

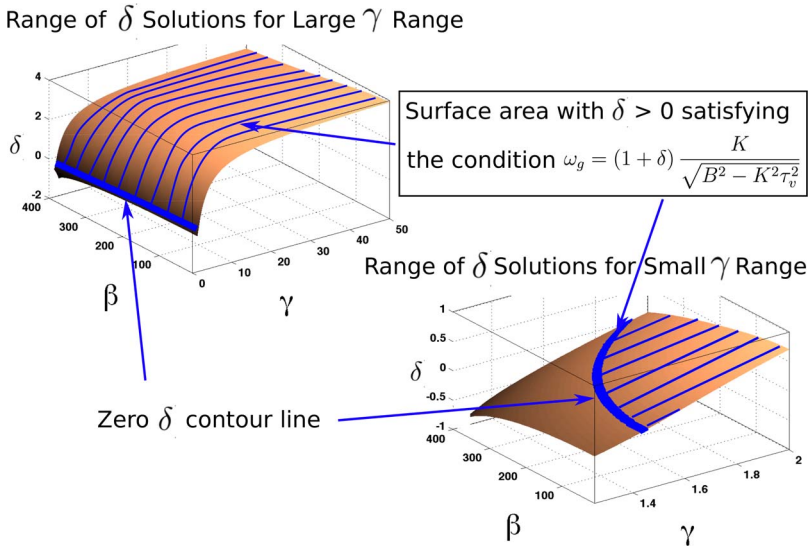

Fig. 5. Controller values meeting the gain crossover sensitivity condition. The surfaces show the range of feedback parameters that meet the gain crossover sensitivity condition of (21). $\delta > 0$ represents the excess gain ratio by which the condition is met. $\gamma > 0$ represents the ratio between damping feedback gain and passive damping. $\beta \in [10, 400]$ is chosen to cover a wide range of actuator parameters. The surfaces demonstrate that a wide range of practical gains γ meet the aforementioned gain crossover sensitivity condition. The values of the surfaces are solved by numerically identifying the smallest real root of (31). In the bottom right surface, it can be seen that $\delta > 0$ for $\gamma > 2$, meaning that the gain crossover sensitivity condition is met if the ratio between damping feedback gain and passive damping is larger than two.

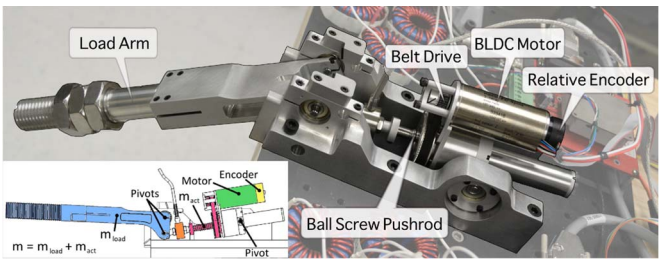

Fig. 6. Linear University of Texas (UT) actuator. This linear pushrod actuator has an effective output inertia of $m = 256$ kg and an approximate passive damping of $b = 1250$ Ns/m.

Identical parameters to the real actuator are used for the simulation, thus allowing us to compare both side by side.

A. Step Response Implementation

First, a test is performed on the actuator, evaluating the response to a step input on its position. The results are shown in the bottom part of Fig. 7, which shows and compares the performance of the real actuator versus the simulated closed-loop controller. All the experimental tests are performed with a 1-kHz servo rate. Additional feedback delays are manually added by using a data buffer. A step input comprising desired displacements between 0.131 and 0.135 m of the physical pushrod length is sent to the actuator. The main reason for constraining the experiment to a small displacement is to prevent current saturation of the motor driver. With very high stiffness, it is easy to reach the 30-A limit for step responses. If current is saturated, then the experiment will deviate from the simulation. The step response is normalized between 0 and 1, for simplicity. Various tests are performed for the same reference input with varying time delays. In particular, large and small delays are used for either or both the stiffness and damping loops. The four combinations of results are shown in the figure with delay values of 1 or 15 ms.

The first thing to notice is that there is a good correlation between the real and the simulated results for both smooth and oscillatory behaviors. Small discrepancies are attributed to unmodeled static friction and the effect of unmodeled dynamics. More importantly, the experiment confirms the anticipated discrepancy in delay sensitivity between the stiffness and damping loops. Large servo delays on the stiffness servo, corresponding to subfigures (a) and (b), have small effects on the step response. On the other hand, large servo delays on the damping servo, corresponding to subfigures (c) and (d), strongly affect the stability of the controller. In fact, for (c) and (d), the results corresponding to $f_n = 12$ Hz are omitted due to the actuator quickly becoming out of control. In contrast, the experiment in (b) can tolerate such high gains despite the large stiffness delay.

B. Distributed Operational Space Control of a Mobile Base

As a concept proof of the proposed distributed architecture on a multiaxis mobile platform, a Cartesian space feedback operational space controller (OSC) [9] is implemented on an omnidirectional mobile base. The original feedback controller was implemented as a centralized process [35], with no distributed topology at that time. The mobile base is equipped with a centralized PC computer running Linux with the RTAI real-time kernel. The PC connects with three actuator processors embedded next to the wheel drivetrains via EtherCAT serial communications. The embedded processors do not talk to each other. The high-level centralized PC, on our robot, has a roundtrip latency to the actuators of 7 ms due to process and bus communications, while the low-level embedded processors have a

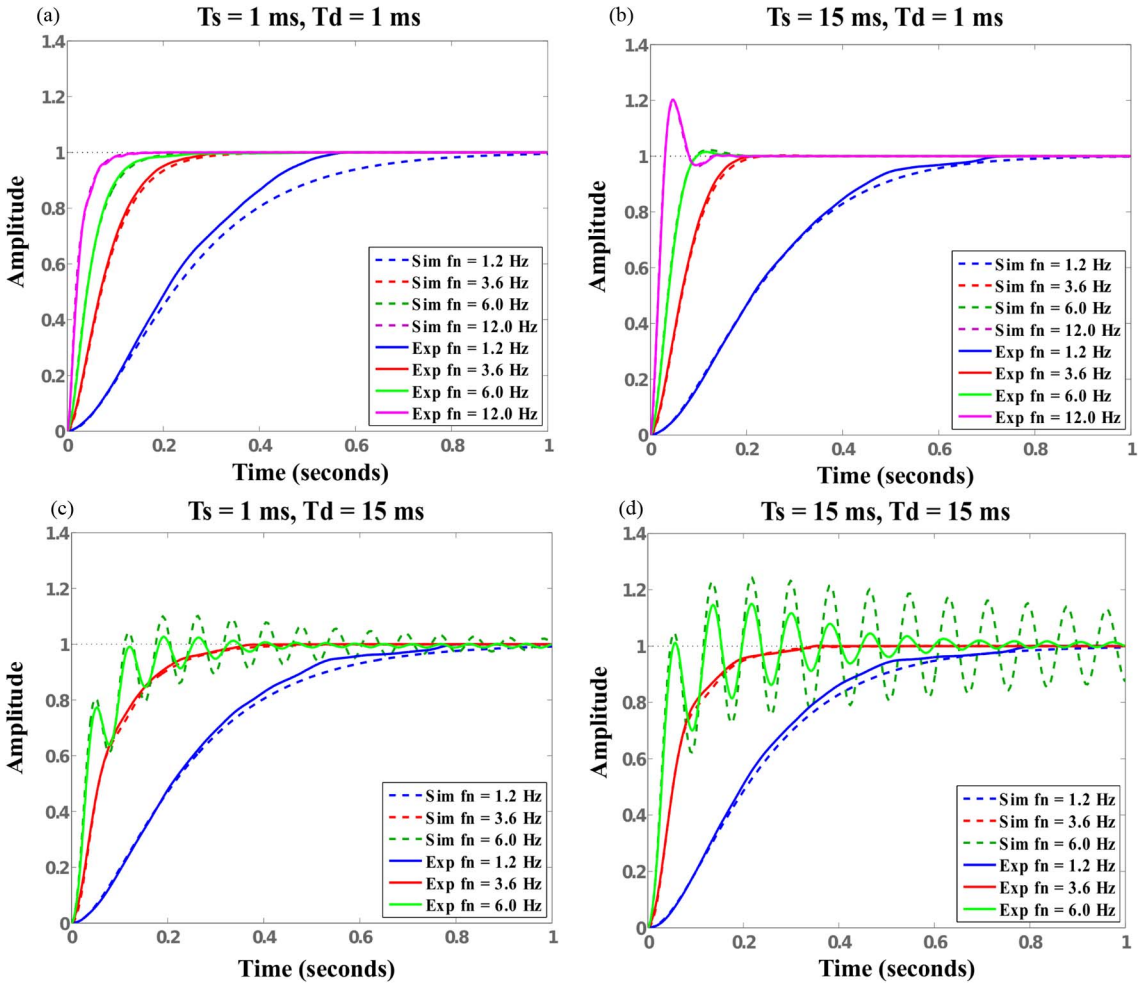

Fig. 7. Step response experiment with the distributed controller. (a) –(d) Various implementations on our linear rigid actuator corresponding to the simulations depicted in Fig. 4. Overlapped with the data plots, simulated replicas of the experiments are also shown to validate the proposed models. The experiments not only confirm the higher sensitivity of the actuator to damping than to stiffness delays but also indicate a good correlation between the real actuator and the simulations.

servo rate of 0.5 ms. Notice that 7 ms is considered too slow for stiff feedback control. To accentuate even further the effect of feedback delay on the centralized PC, an additional 15-ms delay is artificially introduced by using a data buffer. Thus, the high-level controller has a total of 22-ms feedback delay.

An OSC is implemented in the mobile base using two different architectures. First, the controller is implemented as a centralized process, which will be called COSC, with all feedback processes taking place in the slow centralized processor and none in the embedded processors. In this case, the maximum stiffness gains should be severely limited due to the effect of the large latencies. Second, a distributed controller architecture is implemented inspired by the one proposed in Fig. 2 but adapted to a desired OSC, which will be called DOSC. In this version, the Cartesian stiffness feedback servo is implemented in the centralized PC in the same way as in the COSC, but the Cartesian damping feedback servo is removed from the centralized process. Instead, our study implements damping feedback in joint space (i.e., proportional to the wheel velocities) on the embedded processors. A conceptual drawing of these architectures is shown in Fig. 8. The metric used for performance comparison is based on the maximum achievable Cartesian stiffness feedback gains, and the Cartesian position and velocity tracking errors.

To implement the Cartesian stiffness feedback processes in both architectures, the Cartesian positions and orientations of the mobile base on the ground are computed using wheel odometry (more details are discussed in [35]). To achieve the highest stable stiffness gains, the following procedure is followed: 1) first, Cartesian stiffness gains are adjusted to zero, while the damping gains in either Cartesian space (COSC) or joint space (DOSC), depending on the controller architecture, are increased until the base starts vibrating; 2) the Cartesian stiffness gains, on either architecture, are increased until the base starts vibrating or oscillating; 3) a desired Cartesian circular trajectory is commanded to the base, and the position and velocity tracking performance are recorded.

Based on these experiments, DOSC was able to attain a maximum Cartesian stiffness gain of 140 $\mathrm{N}/(\mathrm{m}\cdot\mathrm{kg})$ compared to 30 $\mathrm{N}/(\mathrm{m}\cdot\mathrm{kg})$ for COSC. This result means that the proposed distributed control architecture allowed the Cartesian feedback process to increase the Cartesian stiffness gain (see K_x in Fig. 9) by 4.7 times with respect to the centralized controller implementation. In terms of tracking performance,

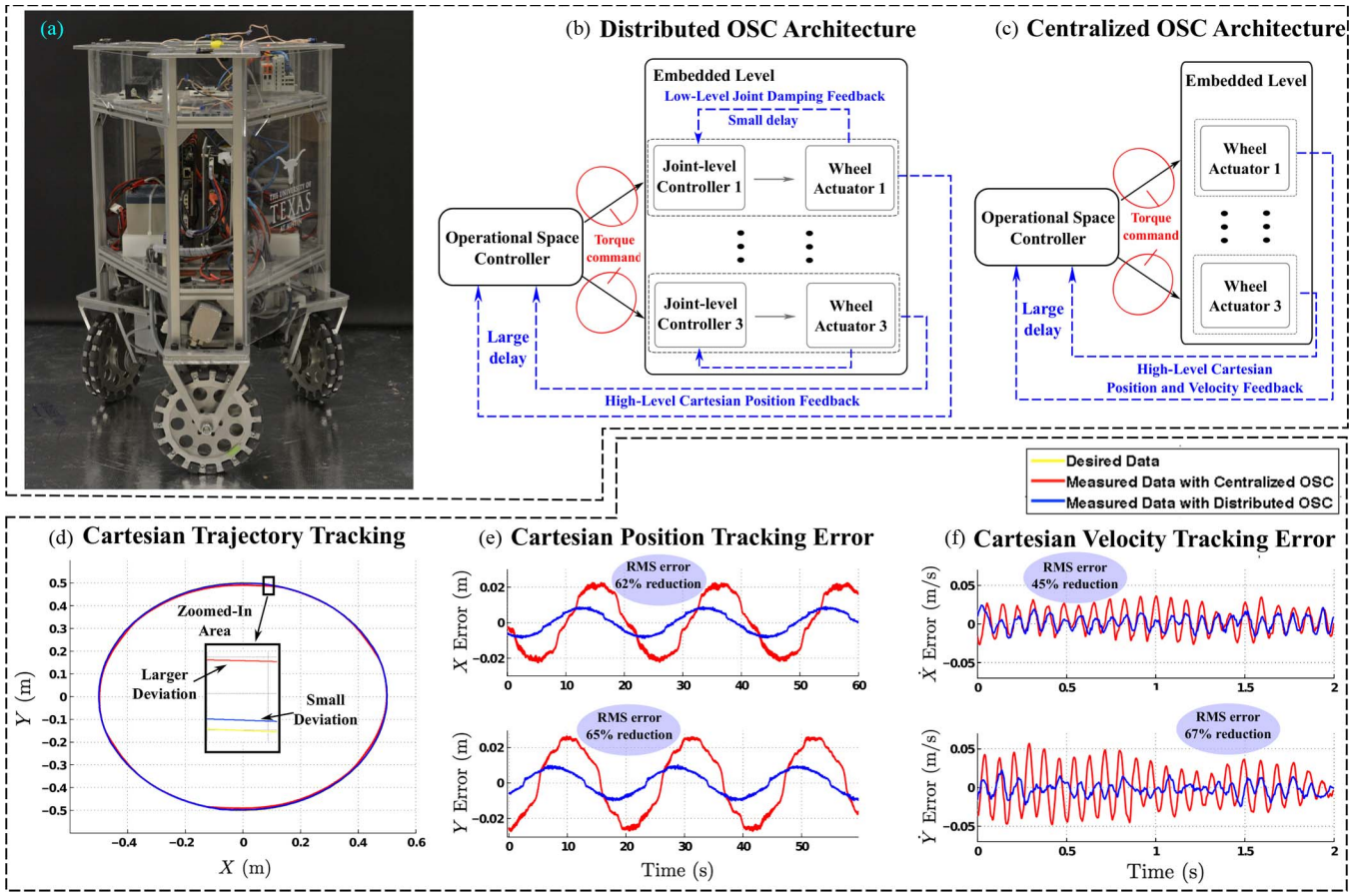

Fig. 8. Omnidirectional mobile base with distributed and centralized OSC controllers. As a proof of concept, we leverage the proposed distributed architectures to our robotic mobile base, demonstrating significant improvements on tracking and stability.

the results are shown in Fig. 8. Both Cartesian position and velocity tracking in DOSC are significantly more accurate. The proposed distributed architecture reduces the Cartesian position root mean error between 62% and 65%, while the Cartesian velocity root mean error decreases between 45% and 67%.

VI. Conclusion and Discussion

The motivation for this paper has been to study the stability and performance of distributed controllers, where stiffness and damping servos are implemented in distinct processors. These types of controllers will become important as computation and communications become increasingly more complex in human-centered robotic systems. The focus has been first on studying the physical performance of a simple distributed controller. Simplifying the controller allows us to explore the physical effects of time delays in greater detail. Then, the proposed architecture has been leveraged to a mobile base system as a proof of concept. Our focus on this paper has been on high-impedance behaviors. This focus contrasts with our previous work on low-impedance control [34]. However, both high- and low-impedance behaviors are important in human-centered robotics. For instance, high-impedance behaviors are important to attain good position tracking in the presence of unmodeled actuator dynamics or external disturbances.

Using the phase margin frequency technique allowed us to reveal the severe effects of delays on the damping loop and appreciate the discrepancy with respect to the stiffness servo behavior. However, to reveal the physical reasons for this discrepancy, an in-depth mathematical analysis is performed based on phase margin sensitivity to time delays. This analysis allowed us to derive the physical condition for the discrepancy between delays. Further analysis revealed that the previous condition is met for high-impedance controllers, in which the damping feedback gain is significantly larger than the passive damping actuator value. To confirm the observations and analytical derivations, two experiments are performed by using an actuator and a mobile base. In particular, the results have shown that decoupling stiffness servos to slower centralized processes does not significantly decrease system stability. As such, stiffness servo can be used to implement OSCs, which require centralized information such as robot models and external sensors.

The next step is to develop a similar study for controllers with an inner torque loop, such as those used for series elastic actuators [34]. For this type of actuators, our interest lies in exploring both high- and low-impedance capabilities (i.e., impedance range) under latencies and using distributed control concepts similar to those explored in this paper. The challenge is that system dynamics become high order instead of second order and more advanced gain selection rules need to be designed for

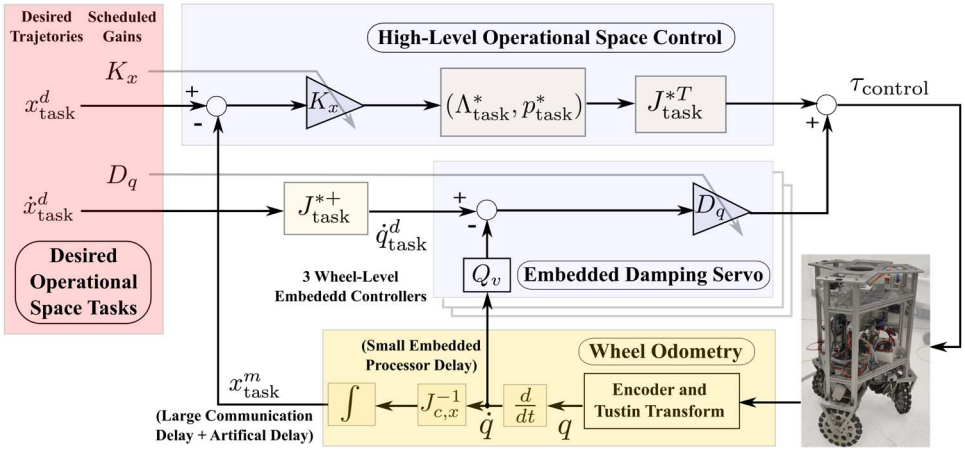

Fig. 9. Detailed distributed operational space control structure. The figure illustrates details of the distributed OSC used for the mobile base tracking experiment. Λ^*_{task} and p^*_{task} are the operational space inertia matrix and gravity-based forces, respectively. J^*_{task} is a contact consistent task Jacobin. More details about these matrices and vectors can be found in [9] and [36]. Our main contribution for this experiment lies in implementing operational space control in a distributed fashion and based on the observations performed on the previously simplified distributed controller. While the high-level operational space stiffness feedback loop suffers from large delays due to communication latencies and artificial delays (added by a data buffer), the embedded-level damping loop increases system stability. As a result, the proposed distributed architecture enables to achieve higher Cartesian stiffness gains K_x for better tracking accuracy.

both impedance and torque gains. Some preliminary results are shown in [37].

Acknowledgment

The authors would like to thank the members of NASA's Software, Robotics and Simulation Division during DARPA's Robotics Challenge Trials, for their great help and support, and the members of the Human Centered Robotics Laboratory at The University of Texas at Austin.

References

[1] N. Paine *et al.*, "Actuator control for the NASA-JSC Valkyrie humanoid robot: A decoupled dynamics approach for torque control of series elastic robots," *J. Field Robot.*, vol. 32, no. 3, pp. 378–396, May 2015.

[2] Y. Sakagami *et al.*, "The intelligent ASIMO: System overview and integration," in *Proc. IEEE/RSJ Int. Conf. Intell. Robots Syst.*, 2002, vol. 3, pp. 2478–2483.

[3] M. A. Diftler *et al.*, "Robonaut 2—The first humanoid robot in space," in *Proc. IEEE Int. Conf. Robot. Autom.*, May 2011, pp. 2178–2183.

[4] A. M. Okamura, "Methods for haptic feedback in teleoperated robot-assisted surgery," *Ind. Robot, Int. J.*, vol. 31, no. 6, pp. 499–508, Dec. 2004.

[5] J.-Y. Kim *et al.*, "System design and dynamic walking of humanoid robot KHR-2," in *Proc. IEEE Int. Conf. Robot. Autom.*, Apr. 2005, pp. 1431–1436.

[6] V. M. Santos and F. M. Silva, "Design and low-level control of a humanoid robot using a distributed architecture approach," *J. Vib. Control*, vol. 12, no. 12, pp. 1431–1456, Dec. 2006.

[7] L. Lu and B. Yao, "A performance oriented multi-loop constrained adaptive robust tracking control of one-degree-of-freedom mechanical systems: Theory and experiments," *Automatica*, vol. 50, no. 4, pp. 1143–1150, Apr. 2014.

[8] J. C. Martin and L. George, "Continuous state feedback guaranteeing uniform ultimate boundedness for uncertain dynamic systems," *IEEE Trans. Autom. Control*, vol. 26, no. 5, pp. 1139–1144, Oct. 1981.

[9] O. Khatib, "A unified approach to motion and force control of robot manipulators: The operational space formulation," *Int. J. Robot. Autom.*, vol. RA-3, no. 1, pp. 43–53, Feb. 1987.

[10] W. Zeng and M. Chow, "A reputation-based secure distributed control methodology in D-NCS," *IEEE Trans. Ind. Electron.*, vol. 61, no. 11, pp. 6294–6303, Nov. 2014.

[11] C. Wang and D. Li, "Decentralized PID controllers based on probabilistic robustness," *J. Dyn. Syst., Meas., Control*, vol. 133, no. 6, 2011, Art. ID. 061015.

[12] G. Cheng *et al.*, "CB: A humanoid research platform for exploring neuroscience," *Adv. Robot.*, vol. 21, no. 10, pp. 1097–1114, 2007.

[13] G. Gu, L. Zhu, Z. Xiong, and H. Ding, "Design of a distributed multiaxis motion control system using the IEEE-1394 bus," *IEEE Trans. Ind. Electron.*, vol. 57, no. 12, pp. 4209–4218, Dec. 2010.

[14] M. Jantsch, S. Wittmeier, and A. Knoll, "Distributed control for an anthropomimetic robot," in *Proc. IEEE/RSJ Int. Conf. Intell. Robot. Syst.*, Oct. 2010, pp. 5466–5471.

[15] A. J. Ijspeert, "Central pattern generators for locomotion control in animals and robots: A review," *Neural Netw.*, vol. 21, no. 4, pp. 642–653, May 2008.

[16] M. Ajallooeian, S. Pouya, A. Sproewitz, and A. J. Ijspeert, "Central pattern generators augmented with virtual model control for quadruped rough terrain locomotion," in *Proc. IEEE Int. Conf. Robot. Autom.*, 2013, pp. 3321–3328.

[17] C.-H. Lee, "A survey of PID controller design based on gain and phase margins," *Int. J. Comput. Cognition*, vol. 2, pp. 63–100, 2004.

[18] K. J. Åström, "Automatic tuning and adaptation for PID controllers—A survey," *Control Eng. Practice*, vol. 1, pp. 699–714, 1993.

[19] E. Poulin, A. Pomerleau, A. Desbiens, and D. Hodouin, "Development and evaluation of an auto-tuning and adaptive PID controller," *Automatica*, vol. 32, no. 1, pp. 71–82, Jan. 1996.

[20] O. Yaniv and M. Nagurka, "Design of PID controllers satisfying gain margin and sensitivity constraints on a set of plants," *Automatica*, vol. 40, no. 1, pp. 111–116, Jan. 2004.

[21] Y. Tipsuwan and M.-Y. Chow, "Gain scheduler middleware: A methodology to enable existing controllers for networked control and teleoperation Part I: Networked control," *IEEE Trans. Ind. Electron.*, vol. 51, no. 6, pp. 1218–1227, Dec. 2004.

[22] J. Y. Lee, M. Jin, and P. H. Chang, "Variable PID gain tuning method using backstepping control with time-delay estimation and nonlinear damping," *IEEE Trans. Ind. Electron.*, vol. 61, no. 12, pp. 6975–6985, Dec. 2014.

[23] J. Colgate and G. Schenkel, "Passivity of a class of sampled-data systems: Application to haptic interfaces," in *Proc. Amer. Control Conf.*, 1994, vol. 3, pp. 3236–3240.

[24] H. Gao, T. Chen, and J. Lam, "A new delay system approach to network-based control," *Automatica*, vol. 44, no. 1, pp. 39–52, 2008.

[25] H. Gao, X. Meng, and T. Chen, "Stabilization of networked control systems with a new delay characterization," *IEEE Trans. Autom. Control*, vol. 53, no. 9, p. 2142, Oct. 2008.

[26] Z.-H. Pang, G.-P. Liu, D. Zhou, and M. Chen, "Output tracking control for networked systems a model based prediction approach," *IEEE Trans. Ind. Electron.*, vol. 61, no. 9, pp. 4867–4877, Sep. 2014.

[27] H. Dong, Z. Wang, and H. Gao, "Distributed h-infinity filtering for a class of Markovian jump nonlinear time-delay systems over lossy sensor networks," *IEEE Trans. Ind. Electron.*, vol. 60, no. 10, pp. 4665–4672, Oct. 2013.
[28] T. Hulin, R. G. Camarero, and A. Albu-Schaffer, "Optimal control for haptic rendering: Fast energy dissipation and minimum overshoot," in *Proc. IEEE/RSJ Int. Conf. Intell. Robot. Syst.*, Nov. 2013, pp. 4505–4511.
[29] S. Yin, X. Li, H. Gao, and O. Kaynak, "Data-based techniques focused on modern industry: An overview," *IEEE Trans. Ind. Electron.*, vol. 62, no. 1, pp. 657–667, Jan. 2015.
[30] S. Yin, S. X. Ding, X. Xie, and H. Luo, "A review on basic data-driven approaches for industrial process monitoring," *IEEE Trans. Ind. Electron.*, vol. 61, no. 11, pp. 6418–6428, Nov. 2014.
[31] N. A. Paine and L. Sentis, "A closed-form solution for selecting maximum critically damped actuator impedance parameters," *J. Dyn. Syst., Meas., Control*, vol. 137, no. 4, 2015, Art. ID. 041011.
[32] K. Ogata and Y. Yang, *Modern Control Engineering*. Englewood Cliffs, NJ, USA: Prentice-Hall, 1970.
[33] Y. Zhao, N. Paine, and L. Sentis, "Sensitivity comparison to loop latencies between damping versus stiffness feedback control action in distributed controllers," in *Proc. ASME Dyn. Syst. Control Conf.*, 2014, pp. 1–10.
[34] N. Paine, S. Oh, and L. Sentis, "Design and control considerations for high-performance series elastic actuators," *IEEE/ASME Trans. Mechatronics*, vol. 19, no. 3, pp. 1080–1091, Jun. 2014.
[35] K. Kim, A. Kwok, and L. Sentis, "Contact sensing and mobility rough and cluttered environments," in *Proc. Eur. Conf. Mobile Robot.*, Sep. 2013, pp. 274–281.
[36] L. Sentis, "Synthesis and control of whole-body behaviors in humanoid systems," Ph.D. dissertation, Dept. Elect. Eng., Stanford Univ., Stanford, CA, USA, 2007.
[37] Y. Zhao, N. Paine, and L. Sentis, "Feedback parameter selection for impedance control of series elastic actuators," in *Proc. IEEE-RAS Int. Conf. Humanoid Robot.*, Nov. 2014, pp. 999–1006.

Ye Zhao (S'11) received the B.E. degree in control science and engineering from Harbin Institute of Technology, Harbin, China, in 2011 and the M.S. degree in mechanical engineering in 2013 from The University of Texas at Austin, Austin, TX, USA, where he is currently working toward the Ph.D. degree in mechanical engineering.

His research interests include impedance control, hierarchical operational space control, series elastic actuation, robust motion planning, and hybrid dynamics of legged locomotion in constrained environments.

Mr. Zhao serves as a Review Editor for *Frontiers in Robotics and AI: Humanoid Robotics*. He is also a Committee Member of the IEEE Robotics and Automation Society (RAS) Technical Committee on Model-based Optimization for Robotics.

Nicholas Paine (S'12) received the B.S., M.S., and Ph.D. degrees from The University of Texas at Austin, Austin, TX, USA, in 2008, 2010, and 2014, respectively, all in electrical engineering.

He is currently a Postdoctoral Researcher with the Human Centered Robotics Laboratory, The University of Texas at Austin. His research interests include design and control of actuators and systems for dynamic legged robots.

Dr. Paine received the Virginia and Ernest Cockrell, Jr. Fellowship in Engineering in 2008.

Kwan Suk Kim (S'15) received the B.S. and M.S. degrees in electrical engineering in 1998 and 2000, respectively, from Sogang University, Seoul, Korea, where he implemented a real-time localization algorithm for an aircraft using a vision sensor. He is currently working toward the Ph.D. degree in mechanical engineering at The University of Texas at Austin, Austin, TX, USA.

He was an Embedded System Software Engineer with LG Electronics Inc. His research interests include safe mobility of humanoid robots and agile skill generation and control for humanoid robots.

Luis Sentis (S'04–M'07) received the M.S. and Ph.D. degrees in electrical engineering from Stanford University, Stanford, CA, USA, where he developed leading work in theoretical and computational methods for the compliant control of humanoid robots.

He worked in Silicon Valley in the area of clean room automation. He is currently an Assistant Professor with The University of Texas at Austin (UT Austin), Austin, TX, USA, where he directs the Human Centered Robotics Laboratory. He was UT Austin's Lead for DARPA's Robotics Challenge entry with the NASA Johnson Space Center in 2013. His research focuses on foundations for the compliant control of humanoid robots, algorithms to generate extreme dynamic locomotion, and building robots for educating students in mechatronics.